Resolving Colocalization of Bacteria and Metal(loid)s on Plant Root Surfaces by Combining Fluorescence in Situ Hybridization (FISH) with Multiple-Energy Micro-Focused X-Ray Fluorescence (ME µXRF)

Linnea K. Honeker[a], **Robert A. Root**[b], **Jon Chorover**[c], and **Raina M. Maier**[d,#]

Linnea K. Honeker: linneah@email.arizona.edu; Robert A. Root: rroot@email.arizona.edu; Jon Chorover: chorover@email.arizona.edu; Raina M. Maier: rmaier@ag.arizona.edu

[a]Department of Soil, Water, and Environmental Science, P.O. Box 210038, University of Arizona, Tucson, AZ, 85721

[b]Department of Soil, Water, and Environmental Science, P.O. Box 210038, University of Arizona, Tucson, AZ, 85721

[c]Department of Soil, Water, and Environmental Science, P.O. Box 210038, University of Arizona, Tucson, AZ, 85721

[d]Department of Soil, Water, and Environmental Science, P.O. Box 210038, University of Arizona, Tucson, AZ, 85721

Abstract

Metal(loid)-contamination of the environment due to anthropogenic activities is a global problem. Understanding the fate of contaminants requires elucidation of biotic and abiotic factors that influence metal(loid) speciation from molecular to field scales. Improved methods are needed to assess micro-scale processes, such as those occurring at biogeochemical interfaces between plant tissues, microbial cells, and metal(loid)s. Here we present an advanced method that combines fluorescence in situ hybridization (FISH) with synchrotron-based multiple-energy micro-focused x-ray fluorescence microprobe imaging (ME µXRF) to examine colocalization of bacteria and metal(loid)s on root surfaces of plants used to phytostabilize metalliferous mine tailings. Bacteria were visualized on a small root section using SytoBC nucleic acid stain and FISH probes targeting the domain Bacteria and a specific group (*Alphaproteobacteria*, *Gammaproteobacteria*, or *Actinobacteria*). The same root region was then analyzed for elemental distribution and metal(loid) speciation of As and Fe using ME µXRF. The FISH and ME µXRF images were aligned using ImageJ software to correlate microbiological and geochemical results. Results from quantitative analysis of colocalization show a significantly higher fraction of As colocalized with Fe-oxide plaques on the root surfaces (fraction of overlap 0.49 ± 0.19) than to bacteria (0.072 ± 0.052) ($p < 0.05$). Of the bacteria that colocalized with metal(loid)s, *Actinobacteria,* known for their metal

[#]Address correspondence to: Raina M. Maier, rmaier@ag.arizona.edu.

tolerance, had a higher correlation with both As and Fe than *Alphaproteobacteria* or *Gammaproteobacteria*. This method demonstrates how coupling these micro-techniques can expand our understanding of micro-scale interactions between roots, metal(loid)s and microbes, information that should lead to improved mechanistic models of metal(loid) speciation and fate.

Graphical Abstract

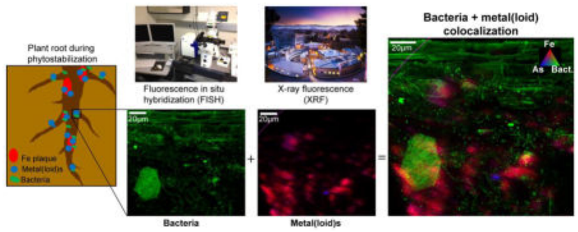

Keywords

Phytostabilization; root-colonizing bacteria; root iron plaques; FISH; iTag sequencing

1 Introduction

Metal(loid)s are naturally present in the environment, but can accumulate above background levels due to agriculture, mining, and other anthropogenic activities, resulting in potential toxicity to surrounding microbial communities and ecosystems. Concentration and bioaccessibility of metal(loid) contamination are routinely measured using bulk geochemical analytical approaches. Similarly, bulk microbiological characterizations can be performed to elucidate microbial community structure and its response to added metal(loid)s. However, tools are lacking that can be used to assess the micro-scale biotic and abiotic interactions that affect bulk-scale biogeochemistry. Such information is needed to better understand both short- and long-term impacts of metal(loid) contamination in the environment as well as remediation outcomes of efforts that seek to stabilize contaminant metal(loid)s in situ rather than remove them. Such technologies include the use of wetlands to treat contaminated water and phytostabilization that seeks to use plants for *in situ* stabilization of metal(loid)s in contaminated soils (Mendez and Maier, 2008; Närhi et al., 2012).

One area where the need for micro-scale information is particularly important to resolving such interactions is the *rhizosphere*, i.e., the plant root surface and the root zone in general. In this zone, root border cells, exudates, and rhizo-deposits promote a 10 to 100-fold increase in the prevalence of bacteria and associated metabolic activity, a process known as the “rhizosphere effect” (Rovira, 1956). Relatively little information is currently available concerning micro-scale root-metal-microbe interactions and the impact on metal(loid) sequestration and transformation. Resolving the intricacies of this micro-environment requires micro-focused methodologies, including scale-appropriate mapping and quantification of both metal(loid)s and microorganisms on the root surface.

For metal(loid) analysis, multiple energy micro-focused x-ray fluorescence imaging (ME μXRF) can be used to identify and create a micro-scale (2 – 500 μm) spatial rendering of metal(loid)s and speciation in a sample. This synchrotron technique can assess the extent of metal(loid) association with a surface as well as the juxtaposition of different metal(loid)s on the surface. For example, this micro-scale technique has been applied in wetland systems to detect As and Pb adsorption to Fe root plaques (Hansel and Fendorf, 2001; Blute et al., 2004; Seyfferth et al., 2011; Zimmer et al., 2011), which are coatings of Fe-oxides formed on a root surface due to oxidation of Fe(II) to Fe(III) as an abiotic process when O_2 is released from the roots, or as a biotic process facilitated by Fe-oxidizing bacteria (FeOB) (St-Cyr et al., 1993; Emerson et al., 1999). Further metal(loid) characterization using x-ray absorption spectroscopy (XAS), which includes x-ray absorption near-edge spectroscopy (XANES) and extended x-ray absorption fine structure (EXAFS), can provide information on metal(loid) oxidation state and local bonding environment, also referred to as molecular speciation. For instance, XRF combined with XAS data indicated As(III) and As(V) juxtaposed with Fe plaques composed primarily of ferrihydrite (ca. 50–100%) with lesser amounts of lepidocrocite (28 ± 1%) on the roots of medium-grained Clarose rice (*Oryza sativa* L., cv. M-206) (Seyfferth et al., 2011). These x-ray techniques can directly measure the chemical speciation of contaminants while also identifying the structure or mineral form of Fe and Mn plaques to help better understand the geochemical processes and cycles, potentially mediated by microbial activities, occurring in discrete locations such as the root zone.

Identification and spatial resolution of bacteria on a micro-scale (2 – 500 μm) can be done using fluorescence in situ hybridization (FISH) in conjunction with 16s rRNA-targeted fluorescent probes and confocal laser scanning microscopy (CLSM). FISH probes can be designed to target different levels of phylogenetic specificity from the domain down to the species level. This technique was first performed on plant roots to quantify and characterize bacterial colonization of wheat roots. Watt et al. (2006) found that most bacteria were situated in biofilm clusters on the root surface with *Pseudomonas* and filamentous bacteria comprising 10% and 4% of all bacteria, respectively. More recently, FISH was adapted for plants grown in mine tailings to study the effects of compost on bacterial colonization of roots (Iverson and Maier, 2009), and it was reported that compost had a positive effect on bacterial colonization, with bacterial root coverage increasing from 3.6 to 18.9% as compost amendment was increased from 0 to 10%. Compared to other methods of analyzing microbial communities in the environment, the benefits of FISH include the ability to spatially and quantitatively resolve microbial communities directly on the root surface.

Here we describe a new method that combines ME μXRF and FISH to allow micro-scale examination, on a single sample, of both metal(loid)s and microorganisms on root surfaces. The method is tested on root surfaces harvested from an on-going phytostabilization study of metalliferous mine tailings to: i) determine its effectiveness for identifying colocalization between particular metal(loid)s and bacteria, and ii) quantify the degree of colocalization in order to evaluate biogeochemical interactions that may contribute to stabilizing metal(loid)s in the root zone. This method can be used to detect either all bacteria or specific groups of bacteria of interest, but the number of different bacterial groups examined in the same sample is limited by the number of fluorescent probe wavelengths available, as will be discussed further. A related approach was employed previously (Mitsunobu et al., 2012) using a combination of EXAFS and FISH to identify iron-oxidizing bacteria associations with geochemical formations on thin sections of natural Fe bio-mats. This group thin-sectioned the bio-mats they were analyzing and then used alternating thin sections for EXAFS or FISH analysis. This allowed inference of bacteria-metal(loid) colocalization by combining results from different thin sections. In the current method we combine FISH with ME µXRF on the same intact section of root surface to directly examine the extent of bacteria and metal(loid) colocalization.

2 Materials and Methods

2.1 Site Description

The Iron King Mine and Humboldt Smelter Superfund (IKMHSS) site, in Dewey-Humboldt, AZ, supported mining operations from 1906 to 1969. Copper, Au and Ag were extracted (Creasey, 1952) leaving behind high concentrations of metal(loid)s including As and Pb, at 3.1 and 2.2 g kg^{-1} respectively (Root et al., 2015). Oxidation of the pyritic tailings in the top 25 cm of the tailings has produced acidic conditions (pH 2.3 – 2.7) (Hayes et al., 2014). Other conditions, including a semi-arid climate, low organic carbon content (0.14 g kg^{-1}), hypersalinity (EC 6.5–9.0 ds m^{-1}) and poor soil structure (Hayes et al., 2014; Valentín-Vargas et al., 2014), cause the surface of the tailings to remain barren and susceptible to wind and water erosion as vehicles for potential contaminant transport. A field trial, initiated in May 2010, is being performed to evaluate the effectiveness of compost-assisted phytostabilization as a remediation technology for the mine tailings (Gil-Loazia et al., 2016). In this study we focus on *Buchloe dactyloides* (buffalograss) roots collected from the treatment containing 15% compost (w/w) (tilled into the top 15 cm of the tailings) seeded with a total of six native plant species, including *B. dactyloides*. The compost amendment had at least five immediate impacts (Valentín-Vargas et al., 2014): 1) the addition of nutrients, 2) the addition of a microbial inoculant more suited to carbon and nitrogen cycling than the resident community, 3) pH neutralization, 4) increased water holding capacity, and 5) improved aggregate structure.

2.2 Sample Collection and Fixation

Three *B. dactyloides* roots were collected from the 15% compost (w/w) field trial plots to be used for both FISH and subsequent ME µXRF analysis. For each root, a different phylum specific probe was used, which is reflected in the sample label: Actino1, Actino2, Alpha1, Alpha2, Alpha3, and Gamma1. For the roots analyzed with the *Actinobacteria* and *Alphaproteobacteria* probes, more than one region of the root was analyzed, as indicated by the numeric part of the label. Roots were collected by cutting off the top of the plant at the surface of the soil and then inserting a corer measuring 2 cm in diameter and 10 cm in length directly over the truncated stem (Valentín-Vargas et al., 2014). Next, a root sample was harvested from the core and treated to fix root-colonizing bacteria by immediately placing it into 4°C, sterile 4% paraformaldehyde (PFA) in phosphate-buffered saline solution (PBS) (7 mM Na_2HPO_4, 3 mM $NaHPO_4$ and 130 mM NaCl, pH 7.2) (Iverson and Maier, 2009). The corer was sterilized with 95% ethanol before each sample collection. The samples were then transported back to the laboratory where they were processed for storage within 12 h of collection. The first step of processing was to remove the root from the PFA and place it into ice-cold sterile PBS. The sample was then shaken vigorously by hand to remove adhered mine tailing particles, and incubated for 10 min. This step was repeated once and then roots were placed into a 1:1 mixture of PBS and 100% ethanol for storage at −20°C (Iverson and Maier, 2009). Four additional *B. dactyloides* root samples and adhered soil were collected from the field for rhizosphere DNA analysis, using the same collection procedure described above and placing the entire soil/root sample from the corer into sterile bags. These samples were kept on ice during transport back to the lab, and then stored at −80°C until DNA extraction.

2.3 Microbial community analysis to determine FISH probes

The choice of FISH probes used to identify root-colonizing bacteria was informed by determining the bacterial phyla that were most abundant in the *B. dactyloides* root zone. Abundance was determined using Illumina sequencing analysis of 16s rRNA gene amplicons (iTags) generated from 4 samples of rhizosphere-influenced soil collected from different locations in the field site. A 0.5 g sample from each collection site was subjected to DNA extraction using the FastDNA Spin Kit for Soil (MP Biomedicals; Santa Ana, CA) following the manufacturer's protocol with some modifications, as outlined in Valentín-Vargas et al. (2014). Library preparation and sequencing were performed at Argonne National Laboratory (Chicago, IL). Library preparation followed a single-step PCR protocol using primers 515f and 806r to amplify V4 region of the 16S rRNA (Caporaso et al., 2012) and sequencing was carried out in a single lane on an Illumina Mi-Seq using v2 chemistry and bidirectional amplicon sequencing (2 × 151bp).

Raw sequence reads were processed using the open source software package QIIME (Quantitative Insights into Microbial Ecology; www.qiime.org). Briefly, forward and reverse reads were joined, requiring a minimum overlap of 30 bp followed by quality filtering using default QIIME parameters and demulitplexing. Default QIIME quality filtering parameters included removing the primer/barcode from the sequence in addition to removing all sequences characterized by a Phred quality score <4, containing any ambiguous (N) base calls, and having a length of <0.75 of original length post quality filtering. After quality filtering, sequences were clustered into operational taxonomic units (OTUs) of greater than or equal to 97% similarity using UCLUST (Edgar, 2010). Representative sequences from each OTU were aligned using PyNAST (Caporaso et al., 2010) and assigned taxonomy using the UCLUST classifier and Greengenes 16S rRNA gene database (DeSantis et al., 2006). Taxonomic results were used to identify the most abundant taxonomic phyla/classes for subsequent development of FISH probes.

Sequence data have been deposited in the NCBI Sequence Read Archive database under the experimental run accession number SRR3476550 as part of BioProject number PRJNA309329.

2.4 FISH

The FISH protocol was adapted from previous studies that performed FISH on roots (Watt et al., 2006; Iverson and Maier, 2009). A fixed root section 10 – 20 mm long and less than 0.2 mm thick was placed onto a quartz slide in the middle of a modified FastWells™ Reagent Barrier (Grace Bio-Labs, CA) with a 1–2 mm section cut-out to enable buffer flow to the root. Low melt agarose (0.2%) was added to keep the root adhered to the slide for the duration of the hybridization process. The slide was then placed in a 37°C hybridization oven (VWR International, PA) until the agarose set, usually about one hour. To dehydrate the root prior to hybridization, the slide was suspended for 3 minutes each in 50, 80, and 98% ethanol.

Probe hybridization was performed in 40 μL of hybridization buffer (HB) (2% 1M Tris-HCl, 18% 5M NaCl, 1 μL 10% SDS, and formamide [see Table 1], in ultrapure deionized [DI] water). All roots received 4 μL of Eub338 mix (20 ng μL^{-1} each of Eub338, Eub338II, and Eub338III) and 4 μL of a group specific probe for either *Actinobacteria* (30 ng μL^{-1} of HGC69a [roots Actino1, Actino2]), *Alphaproteobacteria* (Alf968 [roots Alpha1, Alpha2, and Alpha3]), or *Gammaproteobacteria* (Gam42a [root Gamma1]). Due to the limited number of available channels, constrained by the available fluorophores and corresponding excitation wavelengths as described below, only one group specific probe could be used per root section. For a summary of probe sequences and specific stringencies, see Table 1. All probes sequences are from ProbeBase (Loy et al., 2007) and were designed to target regions of the 16s or 23s rRNA genes. A Hybrislip (Grace Bio-Labs, CA) was placed on each hybridization frame and the entire slide was inserted into a moisture chamber (50 mL centrifuge tube with a Kimwipe saturated with HB) for a 2–2.5 h incubation at 46°C in the hybridization oven After incubation, the Hybrislip was removed so that the root could be rinsed in wash buffer (WB) (2% 1M Tris-HCl, 1% 0.5M EDTA, 5M NaCl [see table 1], and ultrapure DI water) and then the Hybrislip was replaced before immersing the entire slide in a 50 mL tube containing WB and incubating for 15 min in a 48°C water bath. Slides with roots were rinsed in ice-cold ultrapure DI water, dried using compressed air, and then placed in the dark at room temperature until completely dry. Slides were stored in a dark slide box with desiccant at −20°C until viewing.

EDTA is a multi-dentate carboxylate ligand that forms strong complexes with cationic metals, therefore, a small experiment was performed in order to quantify the effects of EDTA, present in the WB, on metal release from the roots. The experiment was performed in triplicate by placing a small section of root, similar to those used in this study, into a microcentrifuge tube containing 1 mL of either ultrapure DI water or 5 mM EDTA. Control treatments containing no root section were also included. Tubes were placed in a 48°C water bath for 15 min, similar to the wash step in the FISH process, and then roots were immediate removed. The remaining liquid was analyzed for Fe and As concentration to assess the extent of metal release from the roots by the Arizona Laboratory for Emerging Contaminants (ALEC) at the University of Arizona in Tucson, AZ. Roots were dried at 40°C for 48 h to obtain a dry weight for normalization of metal release to root mass.

2.5 Confocal Laser Scanning Microscopy (CLSM)

Prior to viewing, slides were allowed to equilibrate to room temperature. As a counterstain, 40 μL of 500 μM SytoBC nucleic acid stain (Molecular Probes, OR) in 10 μM T ris-HCl at pH 8.0 were added to each root and incubated at room temperature for 20 min. This was just long enough for the stain to target nucleic acids within bacterial cells but not long enough for it to permeate plant cells. The counterstain was useful as a control that stained all live and dead bacterial cells on the root and also helped distinguish bacterial cells from background fluorescence in the FISH analysis. SytoBC was rinsed off with 10 µM Tris-HCl and excess liquid was removed by wicking with a Kimwipe and gently blowing with condensed air. The slides were then placed in the dark at room temperature until completely dry.

Once dry, 1 drop of AF1 antifadent mountant (Citifluor Ltd., London) was added to the root and a coverslip (size 1.5, VWR) was carefully placed over the root. Slides were viewed on a Zeiss 510 Meta Confocal Laser Scanning Microscope (CLSM) using a 40x (Plan Apochromat [Apo.] numerical aperture [NA] 1.3) or 63x (Plan Apo. NA 1.4) objective. For viewing SytoBC, CY3 labeled probes, CY5 labeled probes, and autofluorescence, a 488nm Argon laser with a BP 505–570 filter, 543nm HeNe laser with an LP 560 filter, 633 nm HeNe laser with an LP 650 filter, and a 405 nm diode laser with BP 120–480 filter were used, respectively. Autofluorescence was captured with the 405nm laser and later subtracted from all of the other laser lines to reduce overall autofluorescence for image analysis. The captured image consisted of four channels obtained sequentially at each interval and representing a different wavelength. Each probe has a specific excitation and emission wavelength, and the four laser wavelengths and filters listed were optimally chosen to ensure excitation and image collection of the appropriate probe while avoiding any overlap of probe excitation and emission wavelengths. Images were collected at intervals of 1 µm from the surface of the root to a depth that allowed for full outline of root to be depicted, usually about 30 – 50 µm, creating an image stack within each channel. Images were collected from conspicuous regions on the root such as root tips, branching nodes, or protrusions that could be easily re-identified during ME µXRF analysis. To correct for autofluorescence, images were also collected using the 405 nm laser, for subtraction from the other three channels. After viewing, slides were stored at 4°C until transport to the Stanford Synchrotron Radiation Lightsource (SSRL) for ME µXRF analysis.

2.6 Multiple-energy micro-focused x-ray fluorescence imaging (ME µXRF)

Following FISH analysis, ME µXRF imaging across the Fe and As K-edge absorption energies was used to investigate the micron scale (2 µm spot size) spatial distribution of elements, minerals, and chemical species associated with the *B. dactyloides* roots. Similar to the elemental maps that can be collected by scanning electron microscopy (SEM) with energy dispersive x-ray spectroscopy (EDS), high-energy synchrotron-source x-rays can be used to collect images of elemental abundance. Without the necessity for subjecting samples to high vacuum conditions, synchrotron-based XRF data can be collected at near *in situ* conditions with minimal sample preparation or manipulation. Thus, ME µXRF spectromicroscopy is a non-invasive chemical imaging technology that provides elemental and chemical species information at micrometer spatial resolution in a heterogeneous and complex matrix (Jones and Gordon, 1989; Tokunaga et al., 1994; Pickering et al., 2006).

In ME µXRF spectromicroscopy, tuning the incident x-ray energy to exceed core level electron binding energy (e.g., 1S or Kα) of an element of interest results in ionization and creation of a core hole. The core hole is short lived and the subsequent radiative relaxation of a lower energy electron (e.g. e^- transition of L to K) results in a measurable x-ray photon of matching energy. All elements with binding energies below the energy of the incident x-ray will be ionized and emit characteristic x-rays that can be monitored. However, low energy x-rays from low Z elements such as C, N, and O (e.g. $Z < 16$) are attenuated in ambient air, generally not energetic enough to travel to the detector, and therefore are not measured. For an element with an absorption edge sensitive to oxidation state (e.g., As) or interatomic coordination (e.g., Fe), the incident energy of the x-ray can be finely tuned at multiple energies across the absorption edge to exploit the fluorescent response of different species. Stacking the images collected at multiple energies across the absorption edge produces an image of spatially-resolved element speciation, oxidation state, or mineral phase in a complex sample matrix. The normalized fluorescence of the elements with binding energies below the probed element are effectively invariable at the multiple energies across the absorption edge, and speciation analysis is limited to the probed element, e.g., here Fe or As (Root et al., 2015).

X-ray fluorescence imaging of the roots was performed at Beamline 2–3 at the Stanford Synchrotron Radiation Lightsource (SSRL). The bending magnet beamline is optimized for x-ray microprobe analysis with a tunable Si (111) double crystal monochromator that allows for accurate and precise incident x-ray energy calibration with resolution of about 1 eV near the As K-α edge (11867 keV), resulting in distinguishable spectra for different coordination status of iron and arsenic. Images were collected with a 2-μm^2 x-ray probe spot-size achieved with Kirkpatrick-Baez mirrors for focusing optics, stage steps of 2 µm, and 50 ms dwell time per pixel. Fluorescence at each pixel was measured in continuous scanning mode using a single-element silicon drift detector (Vortex, Hitachi) with a multi-channel analyzer (MCA) to bin and calibrate fluorescent counts from isolated elements. Images were collected by rastering the sample on an x-y stage at 45° to the incident x-ray beam (with the detector normal to beam) for optimized fluorescence detection. Coverslips used for confocal microscopy during FISH analysis were removed and excess mountant was wicked away with a Kimwipe, while keeping the root fixed in position on the slide. To assure a representative image in the ME µXRF map, coarse maps up to 1 cm^2 area were collected with large step sizes and short dwell times to assure homogeneity and representative micrographs and aid in the selection of representative points of interest for detailed analysis. The incident x-ray energy was calibrated with Fe and As metal foils with the assigned energy of 7112 eV for the first derivative of the Fe edge, and 11867 eV for the first derivative of the As edge. The ME µXRF images were processed using the analysis toolkit software package SMAK (http://smak.sams-xrays.com). Principal component analysis (PCA) was applied to the 60–80k pixel images to locate regions of unique components or chemical differences (see Mayhew et al., 2011). The unique components highlighted with PCA were probed with micro-focused x-ray absorption near edge structure (µXANES) to confirm the species or mineralogy and analyze the largest variety of different chemical species in the afforded beam-time. The µXANES was at the same spot-size, stage and detector position as image collection.

2.7 Quantitative Analysis of Colocalization

Quantitative analysis of metal(loid)-bacteria spatial overlap, or colocalization, was performed by combining separate FISH and ME µXRF images using ImageJ software

(Schneider et al., 2012). Each original FISH file consisted of four channels composed of image stacks representative of 1 μm intervals of root depth (about 30 – 40 layers) showing fluorescence from the SytoBC live-dead stain, the domain Bacteria probe, a specific group probe, and autofluorescence. To process the original file, it was first split into the four separate channels. Each channel was then compressed from an image stack to a single image representing the entire depth. To correct for autofluorescence, the image representing the background autofluorescence of the root collected with the 405 laser was subtracted from each of the other three images. This resulted in three single images from each original image file: a SytoBC live-dead stain image, a domain Bacteria image, and a specific group (*Actinobacteria*, *Alphaproteobacteria*, or *Gammaproteobacteria*) image.

The three FISH images were then each aligned with a corresponding ME μXRF image (As or Fe). Alignment was required due to parallax from the ME μXRF angle of collection. The plugin TurboReg (Thévenaz et al., 1998) was used for image alignment. TurboReg requires four corresponding landmarks to be selected on each image, such as prominent features on the root, to align one image to the other. Following alignment, the JACoP (Just Another Colocalization Plugin) colocalization tool was used for quantitative analysis (Bolte and Cordelières, 2006). One quantitative measure of the degree of overlap of bacteria-metal(loid) colocalizations on the root are Manders Coefficients M_1 and M_2, where M_1 (Eq. 1) is defined as the ratio of the summed intensities of pixels in which there is a signal from both the bacteria and metal(loid) images to the total intensity of pixels in the metal(loid) image, and M_2 (Eq. 2) is defined conversely for bacteria (Manders et al., 1993).

$$M_1=\frac{\sum_i m_{i,coloc}}{\sum_i m_i} \quad \text{(Eq. 1)}$$

where: $m_{i,coloc}$ = is the colocalization of metal(loid)s and bacteria, m_i = metal(loid)s with no overlap; and

$$M_2=\frac{\sum_i b_{i,coloc}}{\sum_i b_i} \quad \text{(Eq. 2)}$$

where: $b_{i,coloc}$ = is the colocalizatiation of bacteria and metal(loid)s, b_i = bacteria with no metal(loid) overlap. In this case, M_1 represents the fraction of overlap of metal(loid)s with bacteria, and M_2 the fraction of overlap of bacteria with metal(loid)s, each proportional to the amount of per pixel colocalized objects. Coefficients of colocalization can be determined even where the signals from the two components differ strongly (Manders et al., 1993). Because the Manders Coefficient is sensitive to background noise (Bolte and Cordelières, 2006), background evaluation was carefully completed by selecting a region for analysis that did not include empty space and appropriate threshold values were set prior to analysis to adjust for the effects of autofluorescence.

3 Results

3.1 Microbial Community Analysis to Determine FISH Probes

A phylogenetic analysis of the 16S rRNA gene from *B. dactyloides* rhizosphere-associated samples was performed to help choose the probes for FISH analysis. Following Illumina sequencing, a total of 9,600,618 sequences were passed through quality filtering and demulitplexing, after which a total of 8,826,415 sequences remained, of which 481,478 sequences belonged to the *B. dactyloides* rhizosphere-associated samples focused on in this study. Taxonomic classification of OTUs revealed *Proteobacteria* and *Actinobacteria* as the two most dominant phyla in abundances of 42.7 ± 8.0 and 15 ± 5.3% respectively (Fig. 1). The classes *Alphaproteobacteria* and *Gammaproteobacteria* dominated the *Proteobacteria* making up 52.8 ± 4.3 and 33.6 ± 10.0% of this phylum respectively (and 22.4 ± 3.8 and 14.2 ± 4.1% of total abundance). Based on these abundance results, as well as the reported presence of families within these groups that exhibit plant and metal(loid) interactions (see Table 2 for summary), group specific FISH probes were chosen to target *Alphaproteobacteria*, *Gammaproteobacteria*, and *Actinobacteria*.

3.2 FISH

FISH was performed on six *B. dactyloides* roots from the IKMHSS field trail to spatially and phylogenetically characterize bacterial colonization. Representative results are shown in Fig. 2. The section of the root labeled Actino2 that was processed using FISH (and later ME μXRF) is shown in Fig. 2A (white box). SytoBC nucleic acid staining resulted in fluoresence of all cells, both live and dead (Fig. 2B). Conversely, only metabolically active cells were targeted with the domain Bacteria probe Eub338 (Fig. 2C). These images show significant, but incomplete, overlap between the live/dead and metabolically active cells. Cells that fluoresce with the live/dead stain but not the Bacteria probe may be dormant or dead, since probes can only create enough detectable fluorescence in active cells with sufficient ribosomes. Cells targeted by the *Actinobacteria* probe (Fig. 2D) were only a small subset of the live/dead cells shown in Fig. 2B. A prominent *Actinobacteria* colony indicated by the white arrow (Fig. 2D) was also observed with the Syto BC stain (Fig. 2A) and the domain Bacteria probe (Fig. 2B) confirming that this is an actual colony and not autofluorescence. Silicate clay particles can also appear as autofluorescence very strongly with the Syto BC stain (Fig. 2B, **yellow arrow**) and slightly with Eub338 probe (Fig. 2C). However, based on the size and shape of these particles, they are not easily confused with bacterial cells.

Comparable results were observed for roots Actino1, Alpha1, and Gamma1, which were processed for *Actinobacteria*, *Alphaproteobacteria*, and *Gammaproteobacteria*, respectively (Fig. S1). One colony of interest on root Alpha1 is a prominent bacterial colony indicated by the white arrow that is seen both in the SytoBC nucleic acid stained image (Fig. S1H) and with the domain Bacteria probe (Fig. S1I). However, this colony did not hybridize with the *Alphaproteobacteria* probe although *Alphaproteobacterial* cells are visibly distributed over the root surface (Fig. S1J). Additional FISH results for Alpha2 and Alpha3, processed for *Alphaproteobacteria* are shown in Fig. S2.

Roots from similar plants to those used in this study were tested to assess the effects of EDTA (contained in the WB) compared to DI water on metal release from root surfaces. After root addition to plain water, the mass of Fe and As released normalized to the mass of root assayed was 0.56 ± 0.43 μg mg^{-1} and 0.12 ± 0.036, respectively. In comparison, the mass of Fe and As released from roots subjected to a WB rinse containing EDTA, was 2.9 ± 1.6 μg mg^{-1} and 0.14 ± 0.070 μg mg^{-1}, respectively. There was no significant difference between the water and the WB-EDTA treatments and thus, a minimal effect of EDTA on metal release from root surfaces during the FISH process.

3.3. Multiple-energy micro-focused x-ray fluorescence absorption near edge structure

Following FISH analysis, each sample was analyzed by ME μXRF for elemental and mineralogic spatial association. A bicolor map of Fe and As distribution and intensity for root Actino2 (Fig. 2E, 2F) shows abundant Fe plaques (in red) on the root surface with color intensity proportional to relative concentrations; each pixel in the image is 2 μm^2, and the scale bar is 20 μm. Arsenic (shown in blue) is less abundant than Fe and in many areas is present in association with Fe plaques (displayed as purple). Similar results were observed for all other roots examined and other examples can be seen in Fig. S1E, S1K, S1Q, S2E, and S2K.

ME μXRF mapping shows that As is primarily associated with ferric oxyhydroxide coatings at the surface of the roots (Fig 3). It is known that the fluorescent yield varies between elements (O'Day et al., 2004); however, plotting the per pixel fluorescence counts of As versus Fe reveals three distinct stoichiometries of As/Fe co-association (Fig 3C), most pixels having a low As:Fe ratio (ca. 1:60), a few pixels with a high As:Fe ratio (ca. 1:12) and a final set with no observed As. Most of the fluorescence data show a ratio of As:Fe close the mole ratio of As:Fe in the bulk tailings (1:56) (Root et al., 2015). The ME μXRF map for Fe shows a predominance of ferrihydrite with isolated iron silicate clay (chlorite) on the roots. Arsenic is only associated with the areas mapped as ferrihydrite. Areas mapped as chlorite show no colocalized As.

Regions of interest were probed with As and Fe XANES. Iron XANES fine structure is sensitive to Fe-bearing minerals types (O'Day et al., 2004), and As XANES is sensitive to oxidation state (Foster and Kim, 2014). Arsenic XANES spectroscopy confirms that the As on the root surfaces was As(V) (Fig. S5). Two Fe phases were confirmed with μXANES at spots of interest selected based on PCA (Fig. S4): i) a ferrihydrite-like (nominally $Fe(OH)_3$) ferric oxyhydroxide; and ii) a mixed valent Fe-rich clay, matching closely with reference ripidolite [CCa-2 chlorite group; $(Ca_{0.5})(Mg_{4.44},Fe^{[III]}{}_{3.47},Fe^{[II]}{}_{3.02},Al_{0.60},Mn_{0.01},Ti_{0.06})(Si_{4.51},Al_{3.49})O_{20}(OH)_{16}$] (Fig. 3B). The ripidolite reference, from the Clay Mineral Society Source Clay Repository, has diagnostic XANES spectral features that differentiate it from other clay references, and it was identified in the tailings previously (Hayes et al., 2014). The roots were washed prior to ME μXRF analysis suggesting that clay association on the root surface is likely due to root mucilage adhesion. The XANES identified ferrihydrite phase is a ferric (oxy)hydroxide plaque that remained on the root surface after washing, and was not the result of bulk tailings particles.

3.4 FISH/ ME µXRF Quantification and Colocalization

Root coverage by metal(loid)s and bacteria were separately estimated from the ME µXRF and FISH images, respectively (Table 3). Root coverage by Fe (19–20%) on Actino 1, Actino2, and Alpha1 was higher than for the other three roots (4.7–11%). We note that this is possibly due to the region of the root that was examined including: two elongation zones; a broken elongation zone; two lateral root junctions; and a root tip (Table 3). The two intact root elongation zone samples had lower Fe coverage than the other regions examined. In contrast, As coverage varied widely, ranging from 0.6–15% and did not display any patterns related to root region examined. Root coverage estimated from the SytoBC live/dead stain was consistent across all of the roots (6.3 – 8.2%). Analysis of coverage by metabolically active bacteria in comparison to the live/dead bacteria suggests that 20 to 54% of the imaged cells are active (Table 3).

To quantify colocalization between bacteria and metal(loid)s, FISH SytoBC and ME µXRF images were aligned using the imageJ plugin TurboReg (Fig. 2F, S1E, S1K, S1Q, S2E, and S2K). A side by side comparison of the difference between the pre- and post-aligned ME µXRF images is shown in Fig. 2E and 2F, respectively. Alignment of the ME µXRF and FISH images allows direct comparison of metal(loid) and bacterial coverage. Overlays of the SytoBC and ME µXRF images (Figs. 2G, S1F, S1L, S1R, S2F, and S2L) show consistent evidence for colocalization of bacteria with metal(loid) plaques on root surfaces. For example, the white arrow in Fig. 2G points to a prominent *Actinobacteria* colony associated with an Fe/As plaque.

3.4.1 Colocalizing metal(loid) overlap with bacteria—Manders coefficients M_1 and M_2 were calculated from the analysis of aligned FISH - ME µXRF images to quantify colocalization. M_1 and M_2 values represent the fraction of metal(loid) that overlap bacteria and vice versa, respectively, where a value of 1.0 represents complete overlap. Several interesting patterns emerged from this analysis. The fraction of metal overlap with live/dead bacteria (M_1 values) was generally low ranging from 0.015 to 0.13 for Fe and from 0.0040 to 0.17 for As (Fig. 4A and 4B). Examining the overlap that occurred further, both Fe and As generally had higher overlap with all live/dead bacteria than just metabolically active bacteria, suggesting that metal(loid)s are associated with dormant/non-metabolically active cells as well as metabolically active bacteria. Indeed, prior work shows that live and dead cell interactions with (oxyhydr)oxide mineral surfaces are often mediated by strong and kinetically-irreversible covalent bonds formed between surface hydroxylated metal centers (e.g., Fe) and phosphoryl or carboxyl groups of cell surface biomolecules (Parikh and Chorover, 2006 and 2008).

3.4.2 Colocalizing bacterial overlap with metal(loid)s—Examination of fraction of bacterial overlap with metals (M_2 values) showed high variability with values ranging from 0.019 to 0.36 for the association of live/dead bacteria imaged with the Syto BC stain with Fe and values of 0.0010 to 0.37 for As (Fig. 4C and 4D). A striking result from the group specific probes was that *Actinobacteria* consistently had a higher degree of association with Fe than did *Gammaproteobacteria* or *Alphaproteobacteria*. For instance, M_2 coefficients for *Actinobacteria* overlapping with Fe ranged from 0.24 to 0.66, while comparable values were

0.0010 for *Gammaproteobacteria* and 0.019 to 0.27 for *Alphaproteobacteria* (Fig. 4C). We note that in this study, roots that had high Fe coverage (Actino1, Actino2, and Alpha1) also had higher values for both M_1 and M_2 (Fig. 4A and 4C).

3.4.3 Arsenic colocalization with iron vs. with bacteria—Examination of colocalization of As with Fe using all six roots, without consideration of bacteria, showed that the average fraction of overlap of As with Fe plaques was 0.49 ± 0.19. This large association of As with Fe is significantly higher ($p < 0.05$) than the association between As and bacteria which had fraction of overlap values of 0.072 ± 0.052 and 0.053 ± 0.033 with live/dead bacteria and metabolically active bacteria, respectively. This comparison suggests that the primary mechanism of As retention at the root surface is adsorption to Fe plaques rather than to bacterial surfaces.

4 Discussion

Herein we have presented a method that makes conjunctive use of FISH and ME µXRF analyses to characterize the micro-scale associations of bacteria with metal(loid)s on a set of root surfaces grown in arsenic-contaminated, sulfide-ore derived tailings. Applying both techniques to a common set of samples allows discrimination of distinct metal(loid)-bacterial group spatial associations that may reveal insights into biogeochemical mechanisms, such as biomineralization and biodissolution of neo-formed metal(loid)-containing precipitates. Finally, this method allows quantitative analysis of colocalization between metal(loid)s and bacteria on the root surface. Such insights into the association between bacteria and metal(loid)s on root surfaces are needed to develop and test hypotheses concerning the extent to which, and the mechanisms whereby, bacteria and bacterial subgroups are potentially driving metal(loid) transformations.

Several related approaches have been employed previously to examine the micro-scale association of bacteria and metals. One approach used fluorescent probes targeting metals in combination with a nucleic acid stain to assess the colocalization of bacteria, heavy metals, glycoconjugates, and Fe minerals in an aqueous live pure culture using CLSM (Hao et al., 2013; Hao et al., 2016). A drawback to the use of metal-targeting fluorescent probes on a heterogeneous environmental sample is the inability to obtain detailed geochemical and speciation data of the metals present. Furthermore, due to the limited number of fluorescent probe wavelengths available, the number of metals that can be analyzed at the same time is limited. Several research groups have sought to resolve systematic variation in bacterial colonization of geological media using a combination of microbial and geochemical methods on the same samples, as done here. CLSM has been previously combined with synchrotron analysis, particularly scanning laser x-ray microscopy (SLXM), in the study of the structure and metal content of biofilms (Lawrence et al., 2003; Dynes et al., 2006; Neu et al., 2010). Also, a combination of bulk XANES and microbial community analyses (Martínez et al., 2007) as well as micro-scale interrogation of non-specific stained bacterial cells using confocal microscopy (Yoon et al., 2012) was used to describe the biogeochemistry of metalliferous peats. These studies reported indirect evidence for bacterial roles in sulfur reduction with i) a correlation between the presence of *DsrAB* (dissimilatory sulfite reductase) genes, characteristic of sulfur-reducers, and regions of sulfide minerals, such as ZnS (Martínez et al., 2007; Yoon et al., 2012) and ii) confocal microscopy of bacterial cells (stained using a non-specific nucleic acid stain) colocated with presumed sulfide minerals, as detected by autofluorescence (Yoon et al., 2012). The ME μXRF - FISH method described here builds on these techniques by spatially mapping both distinct bacterial cell and metal(loid) types and species, *in situ* on a micro-scale, for direct correlation of bacterial association with neo-formed mineral types. In the present case, the microbial role in biomineralization of arsenic-sequestering Fe plaques in mine tailings was of particular interest, but the data do not provide unequivocal support for a direct microbial role. Rather, they suggest that the root surface itself may govern plaque formation.

Finally, a previous study characterized Pb and Fe (oxyhydr)oxide complexes using EXAFS spectra analysis of Pb-O interatomic distances (Hansel and Fendorf, 2001). Their results showed Pb complexed to an organic substrate with characteristics similar to those exhibited by extracellular polysaccharides (EPS) and/or biofilms, rather than to Fe (oxyhydr)oxides, indicating that Pb^{2+} formed inner-sphere complexes with electronegative oxygen-containing functional groups in biofilm components rather than the Fe-oxide itself. The method used was not able to identify the type of bacteria involved, nor the spatial rendering of interaction. In contrast, results of the current study suggest that direct complexation with biomolecular components is not responsible for most of the As immobilization, an observation that is consistent with both arsenate and most biomolecules exhibiting negative charge. Only a small fraction of As, 0.072±0.052, was spatially-associated with live/dead bacteria. Despite a relatively small proportion of the total As being co-associated with bacteria cells, over large areas this amount can add up; therefore, it would be beneficial to understand the potential role bacteria play in As-immobilization on root surfaces and identify the bacteria that participate in As transformations, such as As-oxidation.

DNA sequencing was used in this study to guide development of the phylum-level probes chosen for FISH-ME μXRF. In addition, these sequence data can be used to help identify populations at greater taxonomic specificity that may be of interest in the system being studied. For example, of the bacterial groups examined, *Actinobacteria* exhibited the highest association with As; overall fraction of overlap values of 0.036 to 0.47 of *Actinobacteria* colocalized with As (Fig. 4D). Within the *Actinobacteria*, the family *Microbacteraceae* had the highest sequence abundance (2.8%). This family contains *Microbacterium lacticum,* a species reported to be capable of As oxidation (Table 2) (Mokashi and Paknikar, 2002). As a second example, we focused on one of the 3 roots probed for *Alphaproteobacteria* which also showed a high association with As (Alpha1; fraction ofoverlap 0.21) (Fig 4D). In examining the *Alphaproteobacteria*, the families *Hyphomicrobiaceae* and *Acetobacteraceae* (present in the rhizosphere at abundances of 2.4 ± 1.6 and 9.0 ± 6.7%, respectively) have been reported to exhibit specific interactions with metal(loid)s (Table 2). For instance, *Acidiphilium multivorum*, of the *Acetobacteraceae* family, is a known As(III) oxidizer (Wakao et al., 1994).

Beyond an apparent lack of direct evidence for a major bacterial role in As sequestration, we also tested for the significance of association between bacteria and Fe plaques on the root surface. This is motivated by the fact that a majority of As was associated with poorly-crystalline Fe(III) plaques (fraction of overlap 0.55 ± 0.15) whose mineralization may be mediated microbially (Banfield et al., 2000), and whose formation gives rise to inner-sphere arsenate surface complexes with well-known stability (e.g., Gao et al., 2013). While the method presented does not prove a bacterial role in plaque formation, it does help to uncover patterns to guide future studies of these roles of bacteria.

The involvement of FeOB in the formation of Fe plaques has been shown previously using acridine orange staining (Emerson et al., 1999) and electron microscopy (St-Cyr et al., 1993). In these studies, bacterial cells were visualized embedded in Fe plaques on roots from aquatic wetland plants. Both studies reported evidence of FeOB after culturing the root tissue; although the cells were not identified *in situ*. However, microbially-mediated aqueous Fe(II) oxidation is not the principal mechanism expected for Fe(III) (oxyhydr)oxide formation in the current system (Hayes et al., 2014). Indeed, extensive presence of iron oxide plaques on root surfaces combined with a relatively low colocalization of bacteria with Fe (fraction of overlap ranges between 0.015 to 0.13 for live/dead bacteria, Fig. 4A) would suggest that, in this particular mine tailings environment, Fe plaque formation may not be a microbiologically-driven process, and plaque nucleation at the root surface is potentially regulated by root surface biomolecules. We recognize, however, that the FISH-ME μXRF data set studied here represents a snapshot in time that cannot rule out the possiblity of previous microbial involvement in the resident Fe root plaque formations, and that fluorescent remnants of microbial cells may have since disappeared. While FeOB-specific probes were not used in this study, DNA sequencing results show that within the phylum *Actinobacteria*, the order *Acidimicrobiales* has a high relative abundance in the rhizosphere of 4.4 ± 2.3% and contains many FeOB species, including *Acidimicrobium ferroxidans*, *Ferrimicrobium acidiphilum,* and *Ferrithrix thermotolerans* (Table 2) (Whitman et al., 2012). One way to address this issue more thoroughly would be to develop a FISH probe for potential FeOB within *Acidimicrobiales*.

While FeOB promote active biomineralization, bacteria may also promote biomineralization passively if surficial biomolecules promote nucleation and crystal growth following adsorption of Fe(III) to cell walls or EPS moeities that complex Fe (Banfield et al., 2000; De Yoreo and Vekilov, 2003). Since a high proportion of *Actinobacteria* were associated with Fe (0.66) (Fig. 4C) we examined the *Actinobacteria* sequences and found that *Acidimicrobiales* contains a species, *Ferrithrix thermotolerans*, capable of Fe-oxide precipitation on its cell surface (Whitman et al., 2012). While colocalization between bacteria and Fe plaques does not necessarily imply a direct bacterial role in Fe plaque formation, the method presented can be used to quantitatively survey potential interactions in development of hypotheses for future studies.

As suggested in the previous paragraphs, one of the next steps in using the FISH-ME μXRF method would be to employ probes designed for specific species hypothesized to play a role in metal(loid) transformations. In addition, a future step could focus on the use of FISH probes that target functional genes in order to detect potential microbial-induced transformations, for instance As oxidation. While traditional FISH, as used in this study, is likely not sensitive enough to target functional genes, catalyzed reporter deposition FISH (CARD-FISH) results in brighter fluorescence and can be used to view functional genes (Pernthaler et al., 2002). Finally, while the analysis done in this study (on roots grown in compost-amended acidic mine tailings in a semi-arid environment) do not provide unambiguous support for a significant bacterial role in metal immobilization, further studies are needed. Repeating the described method in a controlled bench-scale experiment using roots grown in both sterile and non-sterile mine tailing media could help in further elucidating the extent of the role of bacteria in mediating metal transformations and immobilization on root surfaces. Similarly, roots grown in a variety of soils and environmental conditions could assess the effects of factors such as soil type, pH, and TOC content on the factors affecting metal transformations in the root surface.

Other Method Considerations

In order to successfully perform ME μXRF - FISH, there are some important details to consider with respect to the FISH and ME μXRF analyses. Regarding FISH, details to take into account include the limited number of channels available using CLSM (the Zeiss 510 Meta CLSM used in this study has 5), autofluorescence, and possible reagent-induced metal(loid) alterations/loss. The combination of probes used should be carefully selected and optimized due to the limited number of channels available using CLSM. The channels representing the wavelengths 488, 543, and 633 nm used in this study are one optimal combination. Probes should be labeled with fluorphores having the same excitation wavelengths as the channels being used, in order to elicit a fluoresence signal (for a list of fluorphores and corresponding excitation wavelengths see Morrison et al., 2003) and only one probe (or nucleic acid stain) can be used per channel. To overcome these challenges, newer confocal microscopes can have as many as 5 channels. Addtionally, a supercontinuum white light source can be used which generates a continuous spectrum from 450 nm to over 950 nm for the use of mulitple florochromes (Gratton and vandeVen, 2006).

Autofluorescence can present a problem, especially when analyzing root samples because root surfaces and soil particles have the tendancy to autofluoresce. Watt et al. (2006) found that using probes labeled with fluorophores in the far-red spectrum, for instance CY5, provided the least interference by autofluorescence, however, in this study autofluorescence was found to be most problematic using the Bacteria (Eub338) probe labeled with CY5. The Syto BC nucleic acid stain and the specific probes (Gamm42a, Alf968, HGC69a) labeled with CY3 had relatively little autofluroescence (see Fig. 2, S1, and S2). Also, using one wavelength channel that has no associated probes (405 was used in this study) to take an image of the background fluorescence that can later be subtracted from the images taken using the other channels can also be helpful. Though this did not completely remove the autofluorescence in this study, it made a significant improvement in many cases. Finally, it is important to optimize the FISH method for the type of sample being analyzed (i.e., soil, water, mine tailings, rocks, roots, leaves) because different media have varying autofluorescence issues.

Certain reagents used during the FISH process, such as PFA (used to fix roots), and EDTA (present in WB) can potentially alter or promote release of some metal(loid)s. Prior to this study, the effect of PFA on metal(loid) release from the root was examined by measuring the concentration of metal(loid)s from the PFA solution before and after root fixation. There was no significant difference in metal(loid) concentration indicating that metal(loid)s were not released from the root (data not shown). The effects of EDTA, a multi-dentate carboxylate ligand that forms strong complexes with cationic metals, on metal(loid) release from roots were minimized by employing a low (5 mM) concentration. This was verified by conducting a small experiment which showed that there was no significant difference between the Fe and As released after root incubation in 5 mM EDTA compared to water. Furthermore, when using stringencies below 20%, EDTA is not required at all (Daims et al., 2005). Despite these results, it should be recognized that some disturbance and release of metals and/or bacteria likely occur during the extensive processing of the root during fixation and FISH.

With respect to ME μXRF, one major factor to consider when comparing the images to the FISH images is the penetration depth. The depth probed with ME μXRF is controlled by the penetration depth of the incident beam (proportional to the brightness and sample density) and the escape depth of the generated fluorescing x-ray (related to Z and the bulk density). A plant root has relatively low bulk density and is mostly transparent to the incident x-ray. Generally, metal(loid)s of interest can be detected from 100 μm; therefore, the fluorescence of excited metal(loid)s from the full volume of the root exposed to the x-ray is sent to the detector. This makes the distinction of interior versus exterior associations difficult. In the case of the *B. dactyloides* roots used in this study, with diameters of about 100–200 μm, this can lead to an underestimation of M_1 and M_2 values because the FISH confocal image depths only ranged from 30–50 μm. One way to overcome this would be to prepare histological thin-sections of the root before FISH and ME μXRF analysis, so that the same depth is analyzed for both. This is challenging for smaller roots, such as the *B. dactyloides* roots used in this study.

Supplementary Material

Refer to Web version on PubMed Central for supplementary material.

Acknowledgments

We thank Corin Hammond for her dedicated assistance in root analysis at the SSRL. This work was supported by the National Institute of Environmental and Health Sciences (NIEHS) Superfund Research Program (SRP) grant P42 ES04940 and R01 ES1709 and the National Science Foundation Graduate Research Fellowhip Program (NSF GRFP) grant DGE-1143953. Use of the Stanford Synchrotron Radiation Lightsource, SLAC National Accelerator Laboratory, is supported by the U.S. Department of Energy, Office of Science, Office of Basic Energy Sciences under Contract No. DE-AC02-76SF00515.

References

Amann RI, Binder BJ, Olson RJ, Chisholm SW, Devereux R, Stahl DA. Combination of 16S rRNA-targeted oligonucleotide probes with flow cytometry for analyzing mixed microbial populations. Applied and Environmental Microbiology. 1990; 56(6):1919–1925. [PubMed: 2200342]

Banfield JF, Welch SA, Zhang H, Ebert TT, Penn RL. Aggregation-based crystal growth and microstructure development in natural iron oxyhydroxhide biomineralization products. Science. 2000; 289:751–754. DOI: 10.1126/science.289.5480.751 [PubMed: 10926531]

Blute NK, Brabander DJ, Hemond HF, Sutton SR, Newville MG, Rivers ML. Arsenic sequestration by ferric iron plaque on cattail roots. Environmental Science and Technology. 2004; 38(22):6074–6077. DOI: 10.1021/es049448g [PubMed: 15573609]

Bolte S, Cordelières FP. A guided tour into subcellular colocalization analysis in light microscopy. Journal of Microscopy. 2006; 224:213–232. DOI: 10.1111/j.1365-2818.2006.01706.x [PubMed: 17210054]

Caporaso JG, Bittinger K, Bushman FD, DeSantis TZ, Andersen GL, Knight R. PyNAST: A flexible tool for aligning sequences to a template alignment. Bioinformatics. 2010; 26:266–267. DOI: 10.1093/bioinformatics/btp636 [PubMed: 19914921]

Caporaso JG, Lauber CL, Walters WA, Berg-Lyons D, Huntley J, Fierer N, Owens SM, Betley J, Fraser L, Bauer M, Gormley N, Gilbert JA, Smith G, Knight R. Ultra-high-throughput microbial community analysis on the Illumina HiSeq and MiSeq platforms. The International Society for Microbial Ecology Journal. 2012; 6:1621–1624. DOI: 10.1038/ismej.2012.8

Creasey SC. Geology of the iron king mine, Yavapai County, Arizona. Economic Geology. 1952; 47:24–56. DOI: 10.2113/gsecongeo.47.1.24

Daims H, Brühl A, Amann R, Schleifer K, Wagner M. The domain-specific probe EUB338 is insufficient for the detection of all bacteria: Development and evaluation of a more comprehensive probe set. Systematic and Applied Microbiology. 1999; 22:434–444. DOI: 10.1016/S0723-2020(99)80053-8 [PubMed: 10553296]

Daims, H.; Stoecker, K.; Wagner, M. Fluorescence in situ hybridization for the detection of prokaryotes. In: Osborn, AM.; Smith, CJ., editors. Molecular Microbial Ecology. Taylor & Francis Group; New York, NY: 2005. p. 213-239.

De Yoreo JJ, Vekilov PG. Principles of crystal nucleation and growth. Reviews of Mineralogy and Geochemistry. 2003; 54:57–93. DOI: 10.2113/0540057

DeSantis TZ, Hugenholtz P, Larsen N, Rojas M, Brodie EL, Keller K, Huber T, Dalevi D, Hu P, Anderson GL. Greengenes, a chimera-checked 16S rRNA gene database and workbench compatible with ARB. Applied and Environmental Microbiology. 2006; 72:5069–5072. DOI: 10.1128/AEM.03006-05 [PubMed: 16820507]

Dynes JJ, Tylisczak T, Araki T, Lawrence JR, Swerhone GDW, Leppard GG, Hitchcock AP. Speciation and quantitative mapping of metal species in microbial biofilms using scanning transmission x-ray microscopy. Environmental Science and Technology. 2006; 40:1556–1565. DOI: 10.1021/es0513638 [PubMed: 16568770]

Edgar RC. Search and clustering orders of magnitude faster than BLAST. Bioinformatics. 2010; 26:2460–2461. DOI: 10.1093/bioinformatics/btq461 [PubMed: 20709691]

Emerson D, Weiss JV, Megonigal JP. Iron-oxidizing bacteria are associated with ferric hydroxide precipitates (Fe-plaque) on the roots of wetland plants. Applied and Environmental Microbiology. 1999; 65(6):2758–2761. [PubMed: 10347074]

Foster AL, Kim CS. Arsenic speciation in solids using x-ray absorbance spectroscopy. Reviews of Mineralogy and Geochemistry. 2014; 79:257–369. DOI: 10.2138/rmg.2014.79.5

Gao X, Root RA, Farrell J, Ela W, Chorover J. Effect of silicic acid on arsenate and arsenite retention mechanisms on 6-L ferrihydrite: A spectroscopic and batch adsorption approach. Applied Geochemistry. 2013; 38:110–120. DOI: 10.1016/j.apgeochem.2013.09.005 [PubMed: 25382933]

Garrity, GM.; Brenner, DJ.; Krieg, NR.; Staley, JT., editors. Bergey's Manual of Systematic Bacteriology volume 2: The Gammaproteobacteria, part B. Springer; New York: 2005a.

Garrity, GM.; Brenner, DJ.; Krieg, NR.; Staley, JT., editors. Bergey's Manual of Systematic Bacteriology volume 2: The Proteobacteria, part C. Springer; New York: 2005b.

Gil-Loazia J, White SA, Root RA, Solís-Dominguez FA, Hammond CM, Chorover J, Maier RM. Phytostabilization of mine tailings using compost-assisted direct planting: Translating greenhouse results to the field. Science of the Total Environment. 2016; 565:451–461. DOI: 10.1016/j.scitotenv.2016.04.168 [PubMed: 27183459]

Gratton, E.; vandeVen, MJ. Laser sources for confocal micrscopy. In: Pawley, JB., editor. Handbook of Biological Confocal Microscopy. Springer; New York: 2006. p. 21-40.

Hansel CM, Fendorf S. Characterization of Fe plaque and associated metals on the roots of mine-waste impacted aquatic plants. Environmental Science and Technology. 2001; 35:3863–3868. DOI: 10.1021/es0105459 [PubMed: 11642445]

Hayes SM, Root RA, Perdrial N, Maier RM, Chorover J. Surficial weathering of iron sulfide mine tailings under semi-arid climate. Geochemica et Cosmochimica Acta. 2014; 141:240–257. DOI: 10.1016/j.gca.2014.05.030

Hao L, Li J, Kappler A, Obst M. Mapping of heavy metal ion sorption to cell-extracellular polymeric substance-mineral aggregates by using metal-selective fluorescent probes and confocal laser scanning microscopy. Applied and Environmental Microbiology. 2013; 79:6524–6534. DOI: 10.1128/AEM.02454-13 [PubMed: 23974141]

Hao L, Guo Y, Bryne JM, Zeitvogel F, Schmid G, Ingino P, Li JL, Neu TR, Swanner ED, Kappler A, Obst M. Binding of heavy metal ions in aggregates of microbial cells, EPS and biogenic iron minerals measured *in situ* using metal- and glycoconjugates-specific fluorophores. Geochemica et Cosmochimica Acta. 2016; 180:66–96. DOI: 10.1016/j.gca.2016.02.016

Iverson SL, Maier RM. Effects of compost on colonization of roots of plants grown in metalliferous mine tailings, as examined by fluorescence in situ hybridization. Applied and Environmental Microbiology. 2009; 75(3):842–847. DOI: 10.1128/AEM.01434-08 [PubMed: 19047384]

Jones KW, Gordon BM. Trace element determinations with synchrotron-induced x-ray emission. Analytical Chemistry. 1989; 61:341A–358A. DOI: 10.1021/ac00180a001

Krieg, NR.; Staley, JT.; Brown, DR.; Hedlund, BP.; Paster, BJ.; Ward, NL.; Ludwig, W.; Whitman, WB., editors. Bergey's Manual of Systematic Bacteriology. 2. Vol. 4. Springer; New York: 2010.

Lawrence JR, Swerhone GDW, Leppard GG, Araki T, Zhang X, West MM, Hitchcock AP. Scanning transmission x-ray, laser scanning, and transmission electron microscopy mapping of exopolymeric matrix of microbial biofilms. Applied and Environmental Microbiology. 2003; 69:5543–5554. DOI: 10.1128/AEM.69.9.5543-5554.2003 [PubMed: 12957944]

Loy A, Maixner F, Wagner M, Horn M. ProbeBase--an online resource for rRNA-targeted oligonucleotide probes: New features 2007. Nucleic Acids Research. 2007; 35:D800–D804. DOI: 10.1093/nar/gkl856 [PubMed: 17099228]

Manders EMM, Verbeek FJ, Aten JA. Measurement of co-localization of objects in dual-colour confocal images. Journal of Microscopy. 1993; 169(3):375–382. DOI: 10.1111/j.1365-2818.1993.tb03313.x

Manz W, Amann R, Ludwig W, Wagner M, Schleifer K. Phylogenetic oligodeoxynucleotide probes for the major subclasses of Proteobacteria: Problems and solutions. Systematic and Applied Microbiology. 1992; 15(4):593–600. DOI: 10.1016/S0723-2020(11)80121-9

Martínez CE, Yáñez C, Yoon S, Bruns MA. Biogeochemistry of metalliferous peats: Sulfer speciation and depth distributions of dsrAB genes and Cd, Fe, Mn, S, and Zn in soil cores. Environmental Science and Technology. 2007; 41:5323–5329. DOI: 10.1021/es070555v [PubMed: 17822097]

Mayhew LE, Webb SM, Templeton AS. Microscale imaging and identification of Fe speciation and distribution during fluid - mineral reactions under highly reducing conditions. Environmental Science and Technology. 2011; 45(10):4468–4474. DOI: 10.1021/es104292n [PubMed: 21517061]

Mendez MO, Maier RM. Phytostabilization of mine tailings in arid and semiarid environments - an emerging remediation technology. Environmental Health Perspectives. 2008; 116(3):278–283. DOI: 10.1289/ehp.10608 [PubMed: 18335091]

Mitsunobu S, Shiaishi F, Makita H, Orcutt BN, Kikuchi S, Jorgensen BB, Takahashi Y. Bateriogenic Fe(III) (oxyhydr)oxides characterized by synchrotron microprobe coupled with spatially resolved phylogenetic analysis. Environmental Science and Technology. 2012; 46:3304–3311. DOI: 10.1021/es203860m [PubMed: 22360427]

Mokashi SA, Paknikar KM. Arsenic (III) oxidizing *Microbacterium lacticum* and its use in the treatment of arsenic contaminated groundwater. Applied Microbiology. 2002; 34:258–262. DOI: 10.1046/j.1472-765x.2002.01083.x

Morrison, LE.; Ramakrishnan, R.; Ruffalo, TM.; Wilber, KA. Labeling fluorescence in situ hybridization probes for genomic targets. In: Fan, YS., editor. Molecular Cytogenetics: Protocols and Applications. Humana Press; Totowa, NJ: 2003. p. 21-40.

Närhi P, Räisänen ML, Sutinen M, Sutinen R. Effect of tailings on wetland vegetation in Rautuvaara, a former iron-copper mining area in northern Finland. Journal of Geochemical Exploration. 2012; 116–117:60–65. DOI: 10.1016/j.gexplo.2012.03.005

Neef, A. Doctoral thesis. 1997. Anwendung der in situ enzelzell-identifizierung von bakterien zur populationsanalyse in komplexen mikrobiellen biozönosen.

Neu TR, Manz B, Volke F, Dynes JJ, Hitchcock AP, Lawrence JR. Advancing imaging techniques for assessment of structure, composition and function in biofilm systems. FEMS Microbiological Ecology. 2010; 72:1–21. DOI: 10.1111/j.1574-6941.2010.00837.x

O'Day PA, Vlassopoulos D, Root R, Rivera N. The influence of sulfur and iron on dissolved arsenic concentrations in the shallow subsurface under changing redox conditions. Proceedings of the National Academy of Sciences of the United States of America. 2004; 101(38):13703–13708. DOI: 10.1073/pnas.0402775101 [PubMed: 15356340]

Parikh SJ, Chorover J. ATR-FTIR spectroscopy reveals bond formation during bacterial adhesion to iron oxide. Langmuir. 2006; 22:8492–8500. DOI: 10.1021/la061359p [PubMed: 16981768]

Parikh SJ, Chorover J. ATR-FTIR study of lipopolysaccharides at mineral surfaces. Colloids and Surfaces B: Biointerfaces. 2008; 62(2):188–198. DOI: 10.1016/j.colsurfb.2007.10.002 [PubMed: 18006288]

Pernthaler A, Pernthaler J, Amann R. Fluorescence in situ hybridization and catalyzed reporter deposition for the identification of marine bacteria. Applied and Environmental Microbiology. 2002; 68(6):3094–3101. DOI: 10.1128/AEM.68.6.3094-3101.2002 [PubMed: 12039771]

Pickering IJ, Gumaelius L, Harris HH, Prince RC, Hirsch G, Banks JA, Salt DE, George GN. Localizing the biochemical transformations of arsenate in hyperaccumulating fern. Environmental Science and Technology. 2006; 40:5010–5014. DOI: 10.1021/es052559a [PubMed: 16955900]

Roller C, Wagner M, Amann R, Ludwig W, Schleifer K. In situ probing of gram-positive bacteria with high DNA G + C content using 23S rRNA-targeted oligunucleotides. Microbiology. 1994; 140:2849–2858. DOI: 10.1099/00221287-140-10-2849 [PubMed: 8000548]

Root RA, Hayes SM, Hammond CM, Maier RM, Chorover J. Toxic metal(loid) speciation during weathering of iron sulfide mine tailings under semi-arid climate. Applied Geochemistry. 2015; 62:131–149. DOI: 10.1016/j.apgeochem.2015.01.005 [PubMed: 26549929]

Root RA, Vlassopoulos D, Rivera NA, Rafferty MT, Andrews C, O'Day PA. Speciation and natural attenuation of arsenic and iron in a tidally influenced shallow aquifer. Geochimica Et Cosmochimica Acta. 2009; 73:5528–5553. DOI: 10.1016/j.gca.2009.06.025

Rovira AD. Plant root excretions in relation to the rhizosphere effect. Plant and Soil. 1956; 7:178–194. DOI: 10.1007/BF01343726

Schneider CA, Rasband WS, Eliceiri KW. NIH image to ImageJ: 25 years of image analysis. Nature Methods. 2012; 9:671–675. DOI: 10.1038/nmeth.2089 [PubMed: 22930834]

Seyfferth AL, Webb SM, Andrews JC, Fendorf S. Defining the distribution of arsenic species and plant nutrients in rice (*Oryza sative* L.) from the root to the grain. Geochimica Et Cosmochimica Acta. 2011; 75:6655–6671. DOI: 10.1016/j.gca.2011.06.029

St-Cyr L, Fortin D, Campbell PGC. Microscopic observations of the iron plaque of a submerged aquatic plant (*Vallisneria americana michx*). Aquatic Botany. 1993; 46:155–167. DOI: 10.1016/0304-3770(93)90043-V

Thévenaz P, Ruttimann UE, Unser M. A pyramid approach to subpixel registration based on intensity. IEEE Transactions on Image Processing. 1998; 7:27–41. DOI: 10.1109/83.650848 [PubMed: 18267377]

Tokunaga TK, Sutton SR, Bajt S. Mapping of selenium concentrations in soil aggregates with synchrotron x-ray fluorescence microprobe. Soil Science. 1994; 158:421–434. doi: 0.1907/00010694-199415860-00004.

Valentín-Vargas A, Root RA, Neilson JW, Chorover J, Maier RM. Environmental factors influencing the structural dynamics of soil microbial communities during assisted phytostabilization of acid-generating mine tailings: A mesocosm experiment. Science of the Total Environment. 2014; 500–501:314–324. DOI: 10.1016/j.scitotenv.2014.08.107

Wakao N, Nagakawa N, Matsuura T, Matsukura H, Matsumoto T, Hiraishi A, Sakurai Y, Shiota H. *Acidiphilium multivorum* Sp. nov., an acidophilic chemoorganotrophic bacterium from pyritic acid mine drainage. The Journal of General and Applied Microbiology. 1994; 40:143–159. DOI: 10.2323/jgam.40.143

Watt M, Hugenholtz P, White R, Vinall K. Numbers and locations of native bacteria on field-grown wheat roots quantified by fluorescence in situ hybridization (FISH). Environmental Microbiology. 2006; 8(5):871–884. DOI: 10.1111/j.1462-2920.2005.00973.x [PubMed: 16623744]

Whitman, W.; Goodfellow, M.; Kämpfer, P.; Busse, HJ.; Trujillo, ME.; Ludwig, W.; Suzuki, KI.; Parte, A., editors. Bergey's Manual of Systematic Bacteriology volume 5: The Actinobacteria. Springer; New York: 2012.

Yoon S, Yáñez C, Bruns MA, Martínez-Villegas Martínez CE. Natural zinc enrichment in peatlands: Biogeochemistry of ZnS formation. Geochimica Et Cosmochimica Acta. 2012; 84:165–176. DOI: 10.1016/j.gca.2012.01.022

Zimmer D, Kruse J, Baum C, borca C, Laue M, Hause G, Meissner R, Leinweber P. Spatial distribution of arsenic and heavy metals in willow roots from a contaminated floodplain soil measured by X-ray fluorescence spectroscopy. Science of the Total Environment. 2011; 409:4094–4100. DOI: 10.1016/j.scitotenv.2011.06.038 [PubMed: 21762954]

Highlights

- FISH and μXRF are combined to visualize bacteria and metal(loid)s on root surfaces.
- Microscale analysis of bacteria and metal(loid)s reveals potential interactions.
- Co-localization of bacteria and metal(loids) was quantified using ImageJ freeware.
- Phylum-specific FISH probes reveal differing affinity of bacteria for metal plaques.

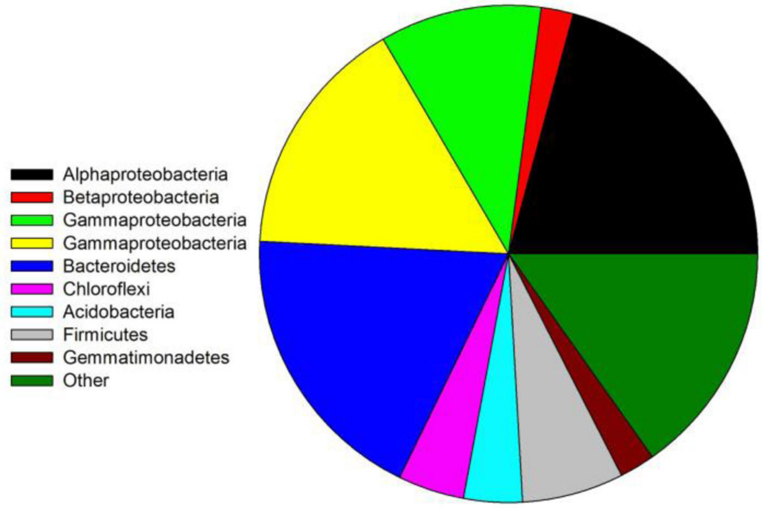

Figure 1.
Average phyla distribution in *B. dactyloides* rhizosphere-influenced mine tailings samples (amended with 15% compost [w/w]; n=4) collected from the IKMHSS field site. DNA was extracted and subjected to 16s rRNA gene amplicon sequencing using Illumina Mi-Seq. Asterisks represent the three largest represented phyla chosen for FISH analysis.

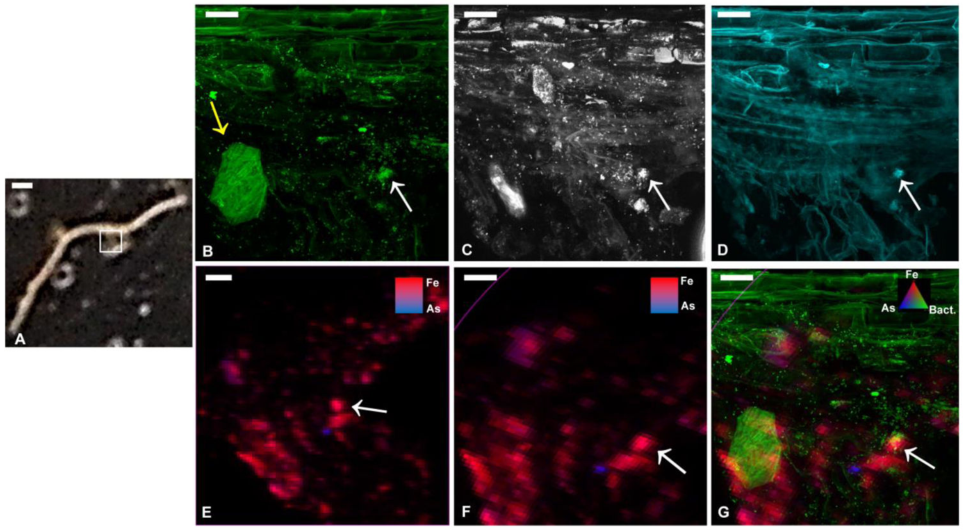

Figure 2.

FISH and ME µXRF images of *B. dactyloides* root Actino2 grown in 15% compost (w/w) amended tailings at IKMHSS. (A) Full root section adhered to slide with white box indicating region of root analyzed for FISH and ME µXRF, (B) all live and dead cells targeted with Syto BC nucleic acid stain, (C) domain Bacteria targeted with a CY5 labeled universal Eub338 mix probe, (D) phylum *Actinobacteri*a targeted with CY3 labeled HGC69a probe, (E) original ME µXRF image showing Fe and As, (F) ME µXRF image after alignment to FISH images using TurboReg plug-in with imageJ, (G) overlay of SytoBC image and aligned ME µXRF image showing colocalization between bacteria and metal(loid)s. White arrow points to a colony of *Actinobacteria* (B, D, G) and corresponding Fe plaque with As (E, F, G). Yellow arrow points to a silicate clay particle on root, visible only with Syto BC stain (B, G). Scale bars represents 500µm in A and 20µm in B–G.

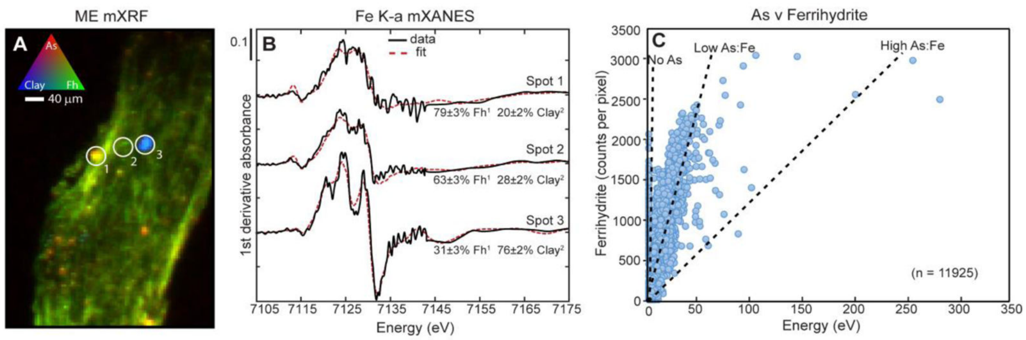

Figure 3.

B. dactyloides root (A) Multiple-energy microfocused x-ray fluorescence (ME µ-XRF) image showing arsenic (in red) associated with a ferrihydrite like ferric hydroxide phase (in green) and areas of iron rich clay, fit as chlorite (in blue, e.g. spot 3) that are not associated with arsenic. The ferrihydrite-like plaque coats the root. The color intensity scale for As, Fe-rich clay (chlorite), and ferrihydrite are 0–50, 0–150, and 0–2500 counts respectively to highlight the As relative to the more abundant ferrous iron. (B) Microfocused (2 µm spot) XANES of select spots on the root were fit to iron minerals, 1Fh = ferrihydrite (synthetic, Root et al., 2009) and 2Clay = chlorite clay (CCa-2, Clay Minerals Society Source Clays Repository, spectra from O'Day et al., 2004), binary fit with standard deviation shown above in panel. (C) Per pixel correlation of As to ferrihydrite, showing regions of high (e.g. spot 1), low (e.g. spot 2) and no arsenic associated with the ferric mineral plaque. Dashed lines in C) point out that some pixels (n=11925 pixels) contain no As, while many pixels have both As and ferrihydrite; at low (1:60) and high (1:12) As:Fe ratios.

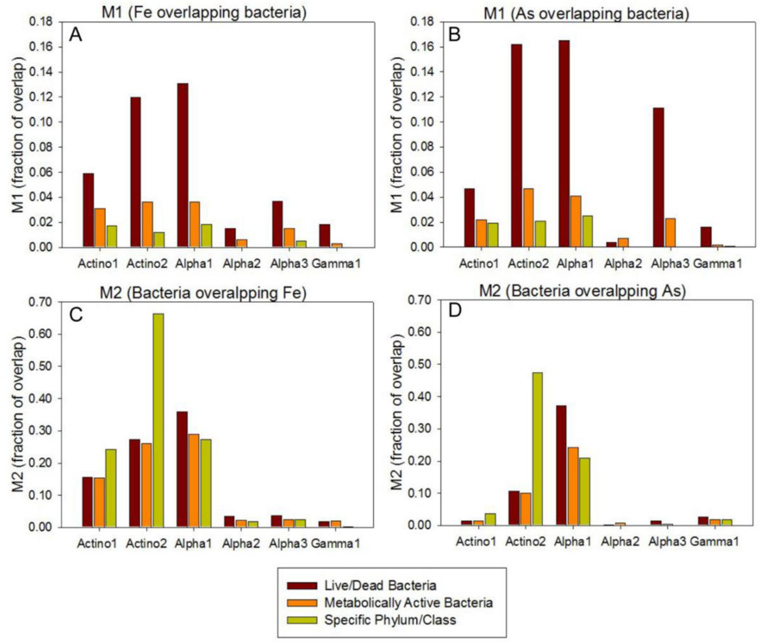

Figure 4.

Manders coefficients (M1 and M2) for overlap of Fe and As with live/dead bacteria, metabolically active bacteria, and specific phyla/classes. (A) M1, representing the fraction of Fe overlapping with bacteria, (B) M1, representing fraction of As overlapping with bacteria, (C) M2, representing the fraction of bacteria overlapping with Fe, (D) M2, representing fraction of bacteria overlapping with As. Note the difference in scales between A and B (M1 values) and C and D (M2 values).

TABLE 1

Domain and group specific probes

Probe name	Target group	Sequence (5′ to 3′)	Stringency (HB[a]/WB[b])	Fluorescent label	Reference
Eub Mix[c]					
Eub338	Domain Bacteria	GCT GCC TCC CGT AGG AGT	Variable	CY5	Amann et al., 1990
Eub338II	*Planctomycetales*	GCA GCC ACC CGT AGG TGT	Variable	CY5	Daims et al., 1999
Eub338III	*Verrucomicrobiales*	GCT GCC ACC CGT AGG TGT	Variable	CY5	Daims et al., 1999
HGC69a	*Actinobacteria*	TAT AGT TAC CAC CGC CGT	25 / 3.0	CY3	Roller eet al., 1994
Alf968	*Alphaproteobacteria*	GGT AAG GTT CTG CGC GTT	20 / 4.3	CY3	Neef, 1997
Gam42a	*Gammaproteobacteria*	GCC TTC CCA CAT CGT TT	35 / 1.4	CY3	Manz et al., 1992

HB, Hybridization buffer; WB, Wash buffer

[a] Formamide in HB (%)

[b] 5M NaCl in WB (%)

[c] EubMix = Eub338 + Eub338II + Eub338III

TABLE 2

B. dactyloides rhizosphere 16S rRNA gene amplicon iTag sequencing results showing families with sequence abundances of ≥1%

		Environments		Interactions with plants			Interactions with metals			
Phylum or Class Order or Family	**Sequence Abundance (%)**	**Metal contaminated**	**Root-colonizing**	**Nitrogen fixing (PGPB)**	**Produce anti-microbials (PGPB)**	**Phyto-pathogenic**	**Accumulate oxidized Fe-Mn deposits**	**S Oxidation**	**Fe Oxidation**	**As(III) Oxidation**
Actinobacteria										
Acidimicrobiales[a]	4.4 ± 2.3	x					x		x	
Cellulomonadaceae[a]	1.0 ±1.4									
Microbacteriaceae[a,b]	1.5 ± 0.2	x				x				x
Geodermatophilaceae[a]	1.0 ± 0.6	x								
Alphaproteobacteria										
Hyphomicrobiaceae[c]	2.4 ± 1.6		x	x (D, N)		x	x			
Sphingomonadaceae[c]	1.9 ± 1.3		x	x (D)						
Acetobacteraceae[c,d]	9.0 ± 6.7	x	x	x (D)				x		x
Caulobacteraceae[c]	2.6 ± 1.7	x								
Gammaproteobacteria										
Sinobacteraceae[e]	6.6 ± 4.0									
Xanthomonadaceae[e]	4.4 ± 2.7				x	x				

PGPB, plant growth promoting bacteria; N, nodulation; D, diazotrophic

[a] from Whitman et al., 2012

[b] from Mokashi and Paknikar, 2002

[c] from Garrity et al., 2005a

[d] from Wakao et al., 1994

[e] from Garrity et al., 2005b

TABLE 3

Percent root coverage by Fe, As, Live/Dead Bacteria, metabolically active bacteria, and specific phyla/class

Root	Region of root	Root Coverage (%)				
		Fe	**As**	**Live/Dead Bacteria**	**Metabolically Active Bacteria**	**Specific Phyla/Class**
Actino1	Elongation zone-broken end	20	2.9	7.8	4.2	1.6
Actino2	Lateral root junction	19	3.5	6.6	1.8	0.21
Alpha1	Root tip	20	15	6.7	2.4	1.6
Alpha2	Lateral root junction	11	3.0	6.3	3.2	0.93
Alpha3	Elongation zone	4.7	0.60	6.9	3.0	1.4
Gamma1	Elongation zone	6.2	8.2	8.2	1.6	1.1